ELSEVIER

Physics of the Earth and Planetary Interiors 94 (1996) 217–239

PHYSICS OF THE EARTH AND PLANETARY INTERIORS

Two-dimensional thermo-kinetic model for the olivine–spinel phase transition in subducting slabs

Rolf Däßler [a,*], Dave A. Yuen [b], Shun-ichiro Karato [c], Michael R. Riedel [a]

[a] *Projectgroup Thermodynamics, University Potsdam, Telegrafenberg C7, 14473 Potsdam, Germany*
[b] *Minnesota Supercomputer Institute and Department of Geology and Geophysics, University of Minnesota, Minneapolis, MN 55415, USA*
[c] *Department of Geology and Geophysics, University of Minnesota, Minneapolis, MN 55455, USA*

Received 2 March 1995; revision accepted 15 August 1995

Abstract

We have investigated the effects of the latent-heat release on the kinetics of the olivine–spinel phase transition to clarify the role of the thermo-kinetic coupling process for the structure of the metastable olivine-wedge in subducting slabs. We have laid out the mathematical formulation of a two-dimensional time-dependent model consisting of the kinetic equations, which are cast as a system of four nonlinear ordinary differential equations (ODE) at each spatial grid point and the time-dependent partial differential equation (PDE) for the temperature, which is coupled to the kinetics by virtue of latent-heat release. This set of ODE–PDE system has been solved by the differential-algebraic method. The structure of the kinetic phase boundary is strongly determined by thermo-kinetic coupling effects during the phase transition. For slow, warm slabs a very narrow phase boundary is obtained near the typical depth for equilibrium phase transformations. From laboratory data we obtain a small latent-heat release (< 10 kJ mol^{-1}), which results in a small heating up of the slab (around 50°). Hence thermo-kinetic coupling effects will not significantly influence the structure of the phase boundary in this regime. For fast, cold slabs narrow regions with metastable olivine may be pushed down to a depth of about 600 km while the thermo-kinetic coupling due to the latent-heat release drastically reduces the depth and the width of the region where olivine and spinel coexist in the cold slab interior. Below the metastable wedge the latent-heat results in a significant and localized heating of the cold slab interior (around 150°), because in this regime the heat release is three times higher. The depth of the metastable wedge in the subducting slab is found to be very sensitive to certain thermodynamic parameters such as the activation energy for growth and the internal slab heating caused by the phase transformation. We propose that deep or intermediate earthquakes occur due to a thermal runaway-effect caused by shear instabilities while these effects are enhanced by the latent-heat release associated with the olivine–spinel transformation. The correlation between fast subducting velocity and the concentration of deep-focus earthquakes at around 600 km depth, as shown for the Tonga–Kermadec trench, can be predicted by this 2-D thermo-kinetic model.

1. Introduction

The role played by phase transitions in mantle dynamics has attracted an increasing amount of

* Corresponding author.

SSDI 0031-9201(95)03103-0

attention in the last several years (e.g. Machetel and Weber, 1991; Honda et al., 1993; Peltier and Solheim, 1992; Steinbach et al., 1993; Tackley et al., 1993). All of these works, however, have only looked at the phase transitions from an equilibrium point of view, in which the transition would follow Clapeyron's relationship between pressure and temperature. The kinetic effects associated with mantle phase transitions and their consequences for mantle dynamics have already been considered by Sung and Burns (1976), Bassett (1979) and later by Goto et al. (1987). Recently there have been experimental (Rubie et al. 1990; Kirby et al., 1991; Brearley et al., 1992; Rubie and Ross, 1994) and theoretical (Morris, 1992) investigations which addressed the problem of phase-transition kinetics in mantle materials, most prominently associated with the olivine to spinel transition. In spite of these advances, a self-consistent model incorporating both the kinetics and thermal fields simultaneously has not been developed, save for the recent numerical models by Däßler and Yuen (1993, 1994). Some studies on thermo-kinetic coupling exists but are related to magma crystallization (Kirkpatrick, 1976; Brandeis et al., 1984; Spohn et al., 1988). Recently an analytical treatment of the thermo-kinetic problem, as applied to magmatic crystallization, has been given in the asymptotic (long-time) limit by Solomatov and Stevenson (1993, 1994).

One of the aims of this paper is to present the thermal-kinetic equations in a formal mathematical manner in order to further future modelling efforts. It is important to put the equations and the boundary conditions within the context of thermo-kinetic interactions at the phase boundary in a mantle-like environment, e.g. with depth-varying temperature and pressure conditions. Another goal of this paper is to investigate the various contributing factors of this highly nonlinear system.

Phase-transition kinetics can have a major role in the generation of deep-focus earthquakes (Green and Burnley, 1989). This has been discussed previously as a possibility by Griggs and Baker (1969) and more recently by Ogawa (1987) but within the context of an equilibrium phase transition. Arguments on the correlation between slab seismicity and phase-change kinetics have been made by Frohlich (1994) and Furukawa (1994). Goto et al. (1987) and Rubie and Ross (1994) have investigated the effects of kinetics and the effects of latent-heat release but did not consider the heat diffusion inside the slab. This work is therefore concerned with the application of a self-consistent two-dimensional thermo-kinetic model to non-equilibrium phase transitions and the consequences for deep-focus earthquakes. This dynamic model is a first approach to describe the long time kinetic behaviour in downgoing slabs, because both the driving force for subduction as well as the transformation faulting process (Kirby et al., 1991) depend on the persistance of metastable olivine inside the slab.

Two-dimensional modelling is needed because in this particular model both the characteristic length scale for temperature variation along the slab and the natural diffusion length scale for transverse variation become comparable. The limitations of the 1-D approach (Däßler and Yuen, 1993) could become significant due to a large latent-heat release during the phase transition. Furthermore, some results from the 2-D thermo-kinetic coupling cannot be obtained in the 1-D modelling, especially in the prediction of the maximum penetration depth of the phase boundary. These intrinsically 2-D phenomenona include the heating of the slab along the longitudinal direction, which will determine for fast slabs the depth at which the transformation occurs.

The plan of this paper is as follows. We will discuss the phase-change kinetic model in Section 2. The thermo-kinetic model in a subducting slab environment and the mathematical formulation for the two-dimensional model will be given in Section 3. We present in Section 4 the results for the temperature fields and the phase boundaries of the coupled system. Section 5 will discuss the ramifications of the results for deep-focus earthquakes. The conclusions and the summary are given in Section 6.

2. Kinetic model

The olivine to spinel phase transitions are first-order transformations, which are usually de-

scribed by a model of simultaneous nucleation and growth processes in a mantle-like environment. Thus martensitic processes are not considered here. The classical homogeneous nucleation and growth theory (Avrami, 1939, 1940, 1941; JMA-theory, Johnson and Mehl, 1939) contains some limitations. For geological purposes the most questionable assumptions are those of a randomly distributed nucleation mechanism and constant rate functions. The kinetics of polymorphic phase transformations have been investigated by previous workers (Hamaya and Akimoto, 1982; Rubie et al., 1990), using the Avrami-equation (Christian, 1965)

$$\xi(t) = 1 - \exp(-kt^n), \tag{1}$$

where $\xi(t)$ is the degree of transformation, n is the Avrami coefficient which determines the nucleation and growth process, k is the rate constant which depends on thermal and mechanical material properties and t is time. For a homogeneous and time-independent nucleation the transformation degree $\xi(t)$ is

$$\xi(t) = 1 - \exp\left(-\frac{\pi}{3} I Y^3 t^4\right), \tag{2}$$

where I is the nucleation rate and Y is the crystal growth rate. Recent experiments show, however, that the rate functions become time-dependent during a phase transition (Carlson, 1983; Rubie et al., 1990) and Eq. (1) cannot be used.

A more general expression for a phase transformation with time-dependent nucleation rate $I[p(t), T(t)]$ and crystal growth rate $Y[p(t), T(t)]$ was formulated by Kirkpatrick (1976):

$$\xi(t) = 1 - \exp - \frac{4\pi}{3} \int_0^t I[p(t'), T(t')] \times \left\{ \int_{t'}^t Y[p(t''), T(t'')]\, \mathrm{d}t'' \right\}^3 \mathrm{d}t' \tag{3}$$

assuming randomly distributed nucleation sites in a spatially homogeneous magmatic melt phase. Hence grain size effects as grain impingement and nucleation site saturation are not explicitly considered in this integral formulation of the transition kinetics. The nucleation rate as a function of temperature T and pressure p is given by (Dowty, 1980)

$$I(p, T) = I_0 T \exp\left(-\frac{\Delta G_t}{RT}\right) \times \exp\left[-\frac{\Delta G^*_{\mathrm{hom}}(p, T)}{kT}\right], \tag{4}$$

and the crystal growth rate as a function of temperature T and pressure p is given by

$$Y(p, T) = Y_0 T \exp\left(-\frac{\Delta G_t}{RT}\right)\left[1 - \exp\left(-\frac{\Delta G_d}{RT}\right)\right], \tag{5}$$

where I_0 and Y_0 are constant pre-exponential factors, $\Delta G^*_{\mathrm{hom}}$ is the free energy for the formation of a stable nucleus, ΔG_t is the free energy for growth, ΔG_d is the free energy difference per unit volume between the different phases or the driving potential, R is the molar gas constant and k is the Boltzmann constant. The free energy for growth ΔG_t becomes depth dependent by including the activation volume V^* (see Sung, 1979) and is given by

$$\Delta G_t = \Delta H_a + pV^*, \tag{6}$$

where ΔH_a is the activation enthalpy for growth.

Table 1 summarizes the terminologies used for describing the phase transition kinetics. For ho-

Table 1
Nomenclature of the physical parameters associated with the phase transition kinetics

Symbol	Meaning
$\Delta G^*_{\mathrm{horn}}$	Free energy for homogeneous nucleation
$\Delta G^*_{\mathrm{het}}$	Free energy for heterogeneous nucleation
ΔG_t	Free energy for growth
ΔG_d	Driving potential
V^*	Activation volume
ΔH_a	Activation enthalpy
ΔQ	Latent-heat release
ΔV	Volume change
σ	Surface tension
ϵ	Strain energy
ΔS	Entropy change
$S(\theta)$	Shape factor
ΔT	Temperature difference
Δp	Excess pressure
I_0	Pre-exponential constant with nucleation rate
Y_0	Pre-exponential constant with growth rate

mogeneous nucleation of spherical nuclei the free energy ΔG^*_{hom} is given by (Christian, 1965)

$$\Delta G^*_{hom} = \frac{16\pi}{3} \frac{\sigma^3 V_m^2}{(\Delta G_d + \epsilon)^2}, \quad (7)$$

where σ is the surface energy and ϵ is the strain energy per unit volume due to the phase mismatch and V_m is the molar volume of olivine. We assume that this strain energy remains small enough to be neglected. The driving force ΔG_d for a phase transformation with both temperature and pressure variation is given by

$$\Delta G_d = -\Delta S \Delta T(p) + \Delta V \Delta p(T), \quad (8)$$

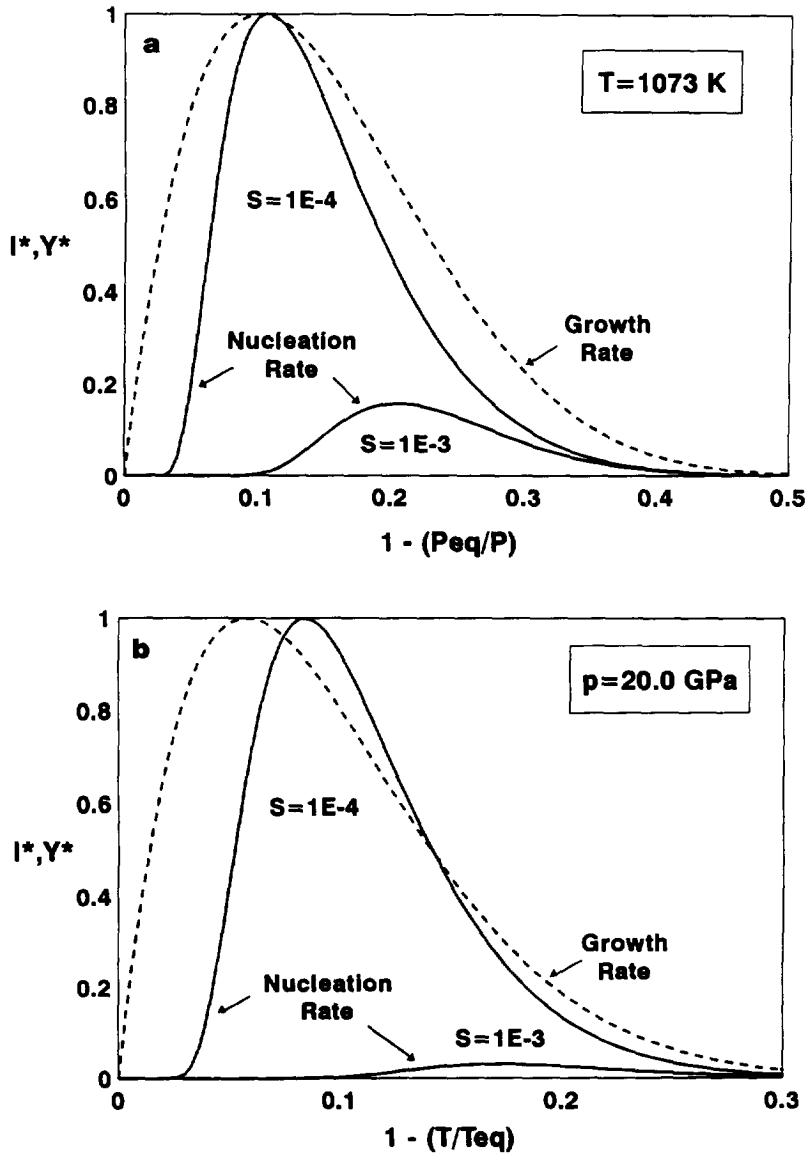

Fig. 1. Dimensionless nucleation and growth rates as a function of the excess pressure (a) at $T = 1073$ K and undercooling (b) at $p = 20.0$ GPa for shape factors of 10^{-3} and 10^{-4}. Growth rates are normalized by their maximum values and nucleation rates by the maximum value for a shape factor of 10^{-4}.

Table 2
Thermodynamic and kinetic parameters of olivine to spinel transition used in the numerical model

Slab thickness D		$7.5 \cdot 10^4$ m
Penetration angle γ		50°
Slab length L		$1.0 \cdot 10^6$ m
Entropy difference ΔS	Akaogi et al., 1989	7.7 J mol^{-1} K^{-1}
Volume change ΔV	Akaogi et al., 1989	$3.16 \cdot 10^{-6}$ m^3 mol^{-1}
Clapeyron constant p_0	Akaogi et al., 1989	10.8 GPa
Molar volume of spinel V_m	Akaogi et al., 1989	$4.05 \cdot 10^{-5}$ m^3 mol^{-1}
Specific heat of olivine c_p	Akaogi et al., 1989	$1.05 \cdot 10^3$ J kg^{-1} K^{-1}
Isothermal bulk modulus k_T	Akaogi et al., 1989	$1.28 \cdot 10^2$ GPa
Surface energy olivine–spinel σ	Rubie et al., 1990	0.6 J m^{-2}
Activation volume V^*	Rubie and Ross, 1994	$6.0 \cdot 10^{-6}$ m^3 mol^{-1}
Thermal diffusivity κ	Jeanloz and Thompson, 1983	$1.0 \cdot 10^{-6}$ m^2 s^{-1}
Adiabatic compressibility β_a	Turcotte and Schubert, 1982	$4.3 \cdot 10^{-3}$ GPa^{-1}
Mantle density ρ_0 at $y = 0$	Turcotte and Schubert, 1982	$3.3 \cdot 10^3$ kg m^{-3}
Thermal expansion α	Griggs, 1972	$3.5 \cdot 10^{-5}$ K^{-1}
Lithospheric base temperature T_L	McKenzie, 1969	1073 K
Number of eigenmodes n	McKenzie, 1969	1000
Pre-exponential constant I_0	Sung and Burns, 1976	$1.0 \cdot 10^{40}$ m^{-3} s^{-1} K^{-1}
Fixpoint growth (15.5 GPa, 1273 K)	Fujino and Irifune, 1992	$3.1 \cdot 10^{-8}$ m s^{-1}

where ΔS is the entropy change, ΔV is the decrease in volume associated with the phase change, ΔT is the undercooling for a transition with a positive Clapeyron slope and Δp is the excess pressure. As a simplification, no deformation processes to result in stress relaxation are taken into account. The equilibrium phase boundary has been calculated from thermodynamic data (Akaogi et al., 1989).

The activation free energy barrier for heterogeneous nucleation is reduced by a shape factor S relative to that for homogeneous nucleation. For a nucleation on grain boundaries the shape factor $S(\theta)$ can be described as a geometrical factor by

$$S(\theta) = \frac{1}{2}(2 + \cos\theta)(1 - \cos\theta)^2, \quad (9)$$

where θ is the wetting angle caused by the different surface tensions (Christian, 1965). The free energy for heterogeneous nucleation ΔG^*_{het} results with

$$\Delta G^*_{het} = S\Delta G^*_{hom}. \quad (10)$$

Fig. 1 shows the nucleation and growth rates for different shape factors as a function of over-

Table 3
Estimates for the maximum nucleation rate, maximum growth rate and maximum grain size, calculated for a kinetic phase boundary of 2–3 km width

Slab velocity w (cm yr^{-1})	Shape factor S	Transition depth y (km)	Activation enthalpy ΔH_a (kJ mol^{-1})	Avrami number Av	Nucleation rate I_{max} (m^{-3} s^{-1})	Growth rate Y_{max} (m s^{-1})	Grain size d (m)
3	10^{-4}	405	400	$6.2\ 10^{14}$	$5.3\ 10^{-7}$	$1.1\ 10^{-14}$	$4.4\ 10^{-2}$
3	10^{-3}	421	400	$3.3\ 10^{15}$	$8.7\ 10^{-9}$	$7.2\ 10^{-14}$	$3.0\ 10^{-1}$
10	10^{-4}	578	450	$1.9\ 10^{19}$	$2.0\ 10^{9}$	$2.1\ 10^{-18}$	$2.6\ 10^{-6}$

pressure (Fig. 1(a)) and undercooling (Fig. 1(b)). The rate functions are calculated from Eq. (4) and Eq. (5) using equilibrium data (Table 2) for the olivine to spinel phase transition. The maxima of the rate functions result from the increase of I and Y due to the increase of the driving potential ΔG_d, which reduces ΔG^*_{het}, while the decrease of I and Y is due to the decrease of the thermal energy with undercooling and the increase of ΔG_t due to the effect of activation volume V^*. From Fig. 1 we can see that the position and the absolute value of the maximum nucleation rate strongly depend on the shape factor, which has been already discussed elsewhere (Sigsbee, 1969). The maxima in Fig. 1 can be used to define the dimensionless rate-functions (Spohn et al., 1988). However, for a kinetic process with both temperature and pressure variation the rate functions were found not to have an absolute maximum in the range of p and T considered. Therefore, we have used for normalization the values of the rate functions I_s and Y_s at a pre-set temperature T_s (1073 K) and a pre-set pressure p_s (20 GPa). Thus maximum rates I_{max} and Y_{max} (see Table 3), which result from the phase transition at lower pressures and temperatures, are much smaller than I_s and Y_s. The dimensionless rate functions are

$$I^* = I/I_s(p_S, T_S) \text{ and } Y^* = Y/Y_s(p_S, T_S). \tag{11}$$

The dimensionless pressure p^* and temperature T^* are normalized by p_S and T_S respectively. The kinetic time scale can be introduced to the scaling of the model for constant rate functions by the Avrami time τ_{Av} (Ave and Yamada, 1986),

$$\tau_{Av} = \frac{1}{\sqrt[4]{I_{max} Y^3_{max}}}. \tag{12}$$

The Avrami number (Spohn et al., 1988) is defined as a dimensionless parameter, which represents the ratio between the kinetic timescale above and the thermal diffusion time τ_{th} of the slab width D given by

$$\tau_{th} = D^2/\kappa, \tag{13}$$

where κ is the thermal diffusivity. Hence it follows that

$$Av = \left(\frac{\tau_{th}}{\tau_{Av}}\right)^4 = \left(\frac{D^2}{\kappa}\right)^4 I_{max} Y^3_{max}, \tag{14}$$

where I_{max} and Y_{max} are the maximum nucleation rates for a typical transformation process (see Table 3). The Avrami number Av characterizes the relative dominance of the kinetics or heat diffusion during the transformation process. Effects of thermo-kinetic coupling can be determined by the value of Av. Furthermore, Eq. (14) determines a critical length scale of instability for Av around 1, e.g. instabilities along the phase boundary are likely to result from thermo-kinetic coupling effects for comparable kinetic and thermal time scales.

3. Numerical model

We have previously constructed a one-dimensional time-dependent model (Däßler and Yuen, 1993) and the system of thermo-kinetic coupling is given there. We now consider a time-dependent 2-D slab model in which the z-coordinate represents the slab length L while the x-coordinate is normal to z (slab width) both normalized by the pre-set and constant slab thickness D. A schematic diagram of the geophysical model used in the numerical calculations is shown in Fig. 2. The y-axis represents the depth which is associated with the z-coordinate by the penetration angle γ. Because of the intensive computational time requirement for obtaining a sufficiently high spatial resolution in the two-dimensional grid, we have employed a slab segment with a length l which is moving down with the slab velocity w. The heat equation is therefore written in Lagrangian framework (coordinate-system $x' - z'$) with time-dependent boundary conditions. In this coordinate system the kinetics for a temporal variation of pressure and temperature are described by a system of 4th order ordinary differential equations in time at each spatial grid point, which portray the evolution of the average grain size $\underline{X} = \{X_3, X_2, X_1, X_0\}^T$. The components (X_3, X_2, X_1, X_0) represent respectively the total

grain volume, total grain area, total grain diameter and number of grains in the extended volume introduced by Avrami (1941). They are obtained by averaging these values with the corresponding crystal size distribution function in configurational space (Riedel and Karato, 1995). The averaging cannot be done in a simple way, because of the time-dependent nucleation and growth process. The resulting system of four coupled ordinary differential equations includes the same physical assumptions as Eq. (3) but is much easier to handle for numerical calculations and allows for the application of solvers for large-scale and stiff problems, such as provided by the differential-algebraic method (Brenan et al., 1989). It is given by

$$\frac{\mathrm{d}}{\mathrm{d}\tau}\begin{bmatrix} X_3(\tau) \\ X_2(\tau) \\ X_1(\tau) \\ X_0(\tau) \end{bmatrix} = \sqrt[4]{Av}\begin{bmatrix} 0 & 4\pi Y^*(\tau) & 0 & 0 \\ 0 & 0 & 2Y^*(\tau) & 0 \\ 0 & 0 & 0 & Y^*(\tau) \\ 0 & 0 & 0 & 0 \end{bmatrix} \cdot \begin{bmatrix} X_3(\tau) \\ X_2(\tau) \\ X_1(\tau) \\ X_0(\tau) \end{bmatrix} + \sqrt[4]{Av}\begin{bmatrix} 0 \\ 0 \\ 0 \\ I^*(\tau) \end{bmatrix}, \tag{15}$$

where τ is the dimensionless time in terms of the thermal diffusion time $\tau = t/\tau_{\mathrm{th}}$. The derivation of Eq. (15) is presented in the appendix. The corresponding degree of volume transformation can be determined by

$$\xi(\tau) = 1 - \exp[-X_3(\tau)], \tag{16}$$

taking into account the grain impingement in a statistical homogeneous medium (Avrami 1939, 1940, 1941). Furthermore the components of X can be used to describe the process kinetics in

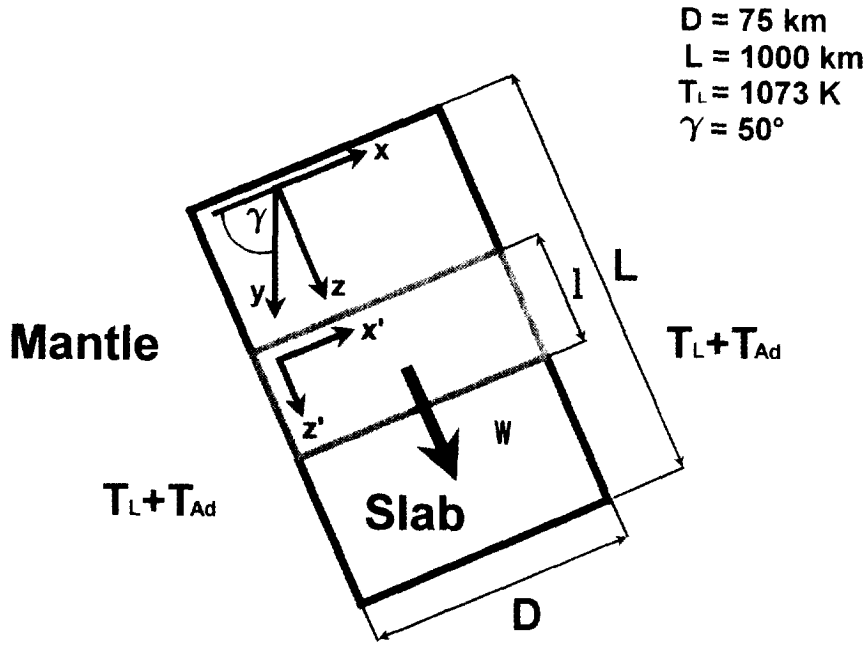

Fig. 2. The two-dimensional slab model used for numerical computation showing the geometry of the system, where z and x are coordinates for the slab length L and the slab width D respectively while the y-axis represents the depth which is associated with the z-axis by the penetration angle γ. For the numerical calculations we consider a downgoing slab segment of the length l (coordinate system $x' - z'$) which is moving with the slab velocity w. T_{L} is the temperature of the surrounding lithospheric base and T_{Ad} is the adiabatic heating.

high-pressure experiments under time varying pressure conditions (Däßler, 1990; Riedel and Däßler, 1990).

The pressure change with time is determined by an ordinary differential equation (ODE) which includes the slab velocity and the volume change of the olivine to spinel phase transition. For simplicity we consider an elastic material without any rheological effects and we assume a constant slab velocity during the subduction process. There are two contributions in the total pressure change with time given by

$$\frac{\mathrm{d}}{\mathrm{d}\tau}p^* = p_0^* + K^* \frac{\mathrm{d}\xi(\tau)}{\mathrm{d}\tau}. \tag{17}$$

The rate of hydrostatic pressure change p_0 represents the pressure change due to the slab penetration in the normalized mantle pressure profile p_M with a velocity w and is given by

$$p_0^* = w^* \frac{\mathrm{d}p_M^*}{\mathrm{d}z^*}. \tag{18}$$

The constant K^* in Eq. (17) is given by the ratio between the relative volume change of the olivine to spinel transition $\Delta V/V$ and the volumetric change from the elastic deformation, with k_T as the isothermal bulk modulus

$$K^* = \frac{\Delta V}{V}\frac{k_T}{p_S}. \tag{19}$$

However, in this study we neglect this pressure change due to the volumetric change, because the stabilizing effect of the pressure decrease during the transformation is found to be very small (Däßler and Yuen, 1993). The mantle pressure p_M varies with the depth y according to the mantle adiabat (Turcotte and Schubert, 1982)

$$p_M(\tau) = -\frac{1}{\beta_a}\ln[1 - \rho_0 g_0 \beta_a y(\tau)], \tag{20}$$

where β_a is the adiabatic compressibility of the mantle, ρ_0 is the mantle density at $y = 0$, and g_0 is the standard gravity. The kinetics are coupled to a two-dimensional partial differential equation (PDE) for the heat transfer, written in the Lagrangian frame of reference, moving with the slab velocity

$$\frac{\partial T^*}{\partial \tau} = \frac{\partial^2 T^*}{\partial x'^2} + \frac{\partial^2 T^*}{\partial z'^2} + S_1 \frac{\mathrm{d}\xi(\tau)}{\mathrm{d}\tau} + T_{ad}^* w^* \cos\gamma, \tag{21}$$

where w^* is the normalized slab velocity, γ is the penetration angle and T_{ad}^* is the adiabatic heating. The heat Eq. (21) contains both terms of the latent-heat release and adiabatic heating. The Stefan number S_1 represents the ratio between the latent-heat release ΔQ and the characteristic internal energy $c_p T_S$, where c_p is the specific heat of olivine,

$$S_1 = \frac{\Delta Q}{c_p T_S}. \tag{22}$$

The latent heat ΔQ released per mole of olivine (Akaogi et al., 1989; Rubie and Ross, 1994) is given for non-equilibrium phase changes by

$$\Delta Q = \Delta H_{T,p_{equ}} + \int_{p_{equ}}^{p} \Delta V(p', T)\,\mathrm{d}p', \tag{23}$$

where we assume $\Delta V(p', T)$ to be constant. The pressure dependence of the latent-heat release results from the difference in the free energy ΔG of the olivine and spinel phase in the non-equilibrium case. At about 600 km depth the latent-heat release can be three times higher than near the typical depth of the equilibrium phase transition (see value for $\Delta V(p', T)$ in Table 2). The adiabatic heating T_{ad} is given (Griggs, 1972) by

$$T_{ad} = \int_0^y \frac{\alpha(T, p) g T}{c_p}\,\mathrm{d}y', \tag{24}$$

where $\alpha(T, p)$ is thermal expansion coefficient. In the depth range beween 300 km and 700 km we use a linear approximation of pressure dependence of the thermal expansion coefficient α (Griggs, 1972).

$$\alpha(y)[\mathrm{K}^{-1}] = 3.5 \cdot 10^{-5}[\mathrm{K}^{-1}] - y \cdot 0.25 \cdot 10^{-10}[\mathrm{m}^{-1}\mathrm{K}^{-1}]. \tag{25}$$

The adiabatic heating influences the initial temperature profile as well as the boundary con-

ditions. However, the effects of adiabatic heating as a heat source during the transition kinetics are rather small compared to the latent-heat release. The initial temperature inside a descending slab in the Eulerian framework is given by (McKenzie, 1969)

$$T(\tau=0) = T_c + (T_L - T_c)\left\{1 + 2\sum_n \frac{(-1)^n}{n\pi} \times \exp\left[\left(R_e - \left(R_e^2 + n^2\pi^2\right)^{0.5}\right)x^*\right] \times \sin(n\pi z^*)\right\}, \quad (26)$$

where T_c (273 K) is the constant surface temperature, T_L (1073 K) is the constant temperature for the base of the lithosphere on the assumption of no interaction between mantle and descending slab, R_e is the thermal Reynolds number which depends on the slab velocity and n is a positive integer.

The thermal boundary conditions along both sides of the slab segment are implemented by including both the lithospheric basal temperature T_L and the adiabatic heating T_{ad} which varies with depth

$$T(\tau, z', x' < 0) = T(\tau, z', x' > D) = T_L + T_{ad}(\tau). \quad (27)$$

These side boundary conditions are employed for both slow and fast subducting slabs. The implementation of the boundary conditions along the bottom and the top of the slab segment is much more problematic because these boundary conditions can strongly influence the temperature field inside a small slab segment. Assuming much faster kinetics as compared with the heat flux we expect a small thermal interaction along the boundary. Therefore we use adiabatic conditions at the top and the bottom of the slab segment. Hence the temperature field can be influenced by earlier events of heat release during the subduction process. A more realistic simulation would involve the calculation of the thermal evolution inside the whole slab from the beginning of the penetration into the mantle until the present

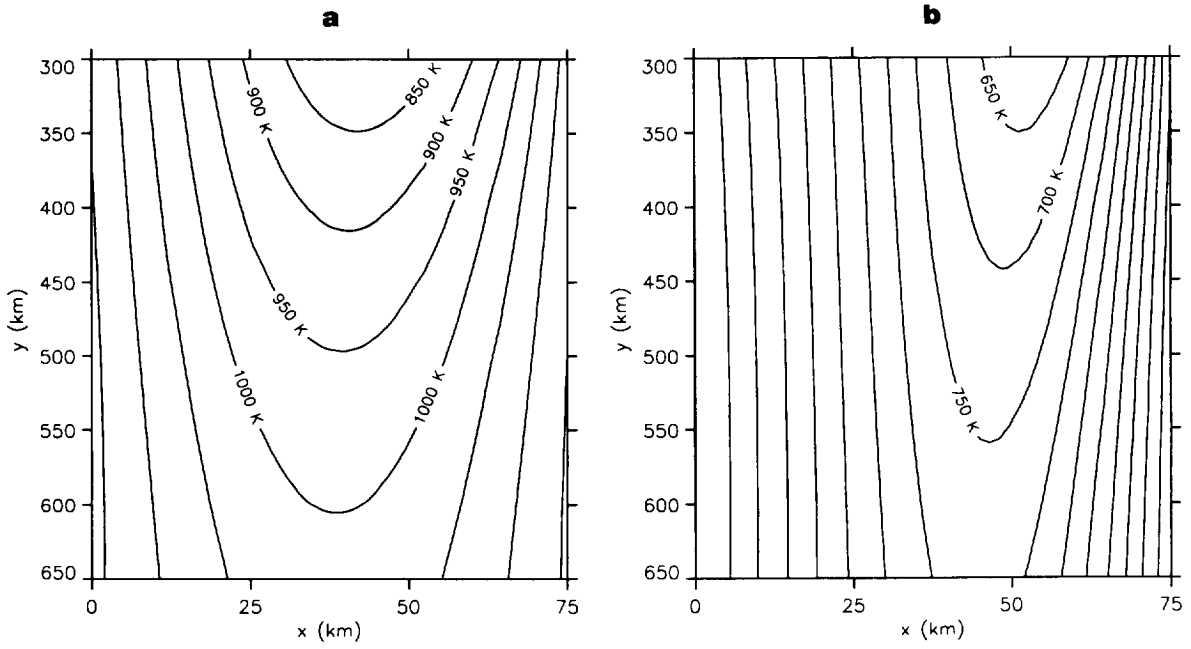

Fig. 3. Two-dimensional initial temperature fields inside subducting slabs without any heat source for (a) slow (w = 3 cm yr^{-1}) and (b) fast (w = 10 cm yr^{-1}) regimes both for a penetration angle of 50°. The temperature fields (labels in K) result from Eq. (26). The depth scale here and in the following is given for the centre of the slab at x = 37.5 km.

time. However, recent kinematic slab models (Minear and Toksöz, 1970; Hsui and Toksöz, 1979; Goto et al., 1987) do not give a sufficiently high spatial resolution to obtain these particular thermo-kinetic coupling effects.

Two-dimensional temperature fields inside downgoing slabs without any heat source are shown in Fig. 3 both slow and fast slabs. The characteristic temperature fields result from the initial temperature Eq. (26). For slow velocities (Fig. 3(a)) the slab is heated up while for fast slab velocities (Fig. 3(b)) the slab interior remains cold deep in the mantle. The velocity dependence of the temperature is controlled by the thermal Reynolds number. The effect of adiabatic heating generally increases the temperature with increasing depth, while the amount of adiabatic heating sensitively depends on the thermal expansivity. The asymmetric temperature fields result from the initial temperature field inside the oceanic lithosphere before the subduction process. From Fig. 3 we construct adiabats T_a for the coldest region of the slab interior and different slab velocities. These adiabats are used to show different paths of the kinetic p–T-diagrams in Fig. 4.

Both the temperature equation (Eq. (21)) and the ODE-system (Eqs. (15) and (16)) are solved numerically by the differential algebraic method (DASPK), which was developed for large-scale stiff systems in both space and time (Brenan et al., 1989; Maier and Petzold, 1993). The solving algorithm allows for the treatment of a coupled PDE and ODE system and includes iterative methods with variable stepsizes in time. Up to 100 gridpoints with a corresponding spatial resolution of about 0.7 km have been employed in the spatial discretization in both directions. This problem is numerically very stiff and requires small steps because of the different timescales present in the coupled thermo-kinetic system. All calculations were done with a constant slab width D of 75 km and a constant penetration angle of

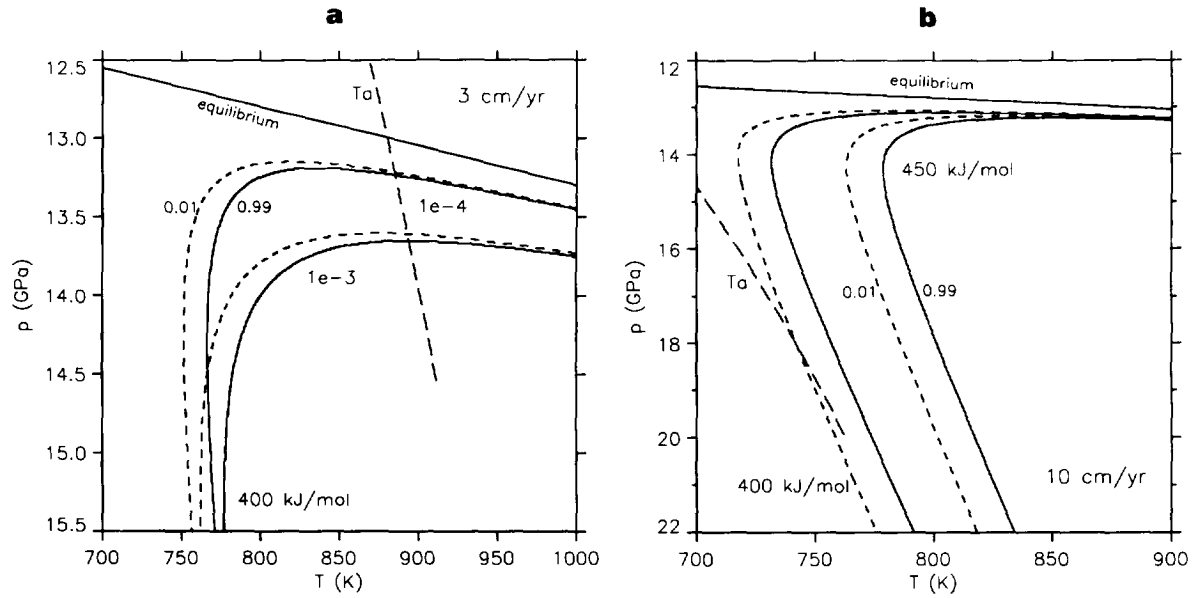

Fig. 4. p–T-diagrams containing the kinetic phase boundaries of the olivine to spinel transition for different slab velocities without any heat diffusion. The isolines mark the transformation regions between $\xi = 0.01$ (dashed line) and $\xi = 0.99$ (solid line). Adiabats (T_A) (see Fig. 3) for a slab velocity of 3 cm yr^{-1} and 10 cm yr^{-1} are crossing the kinetic phase boundaries. The kinetic phase boundaries are shown for different shape factors (10^{-}u3 and 10^{-4}) in the slow regime (a) and for the different activation enthalpies ΔH_a (400 kJ mol^{-1} and 450 kJ mol^{-1}) in the fast regime (b).

50°, characteristic for subducting slabs, while the dependence of the plate thickness on the subduction age is not considered here.

The thermodynamic parameters for the olivine to spinel phase transition which are kept constant in the numerical computation are given in Table 2. Most of the thermodynamical data are taken from experiments with forsterite (Akaogi et al., 1989). The pre-exponential factor for nucleation I_0 in Eq. (4) is set to be 10^{40} m^{-3} s^{-1} K^{-1} according to some theoretical estimates (Sung and Burns, 1976) while the exponential prefactor for growth Y_0 in Eq. (5) varies with ΔH_a to be consistent with growth rates obtained in recent experiments. To reduce the number of free parameters, we used as a fixpoint for the growth rate $3.1 \cdot 10^{-8}$ m s^{-1} at 15.5 GPa and 1273 K (Fujino and Irifune, 1992). The calibration of the pre-exponential factor Y_0 with ΔH_a between 350 kJ mol^{-1} and 450 kJ mol^{-1} is given by

$$Y_0[\mathrm{m\,s^{-1}\,K^{-1}}] = 1.0[\mathrm{m\,s^{-1}\,K^{-1}}] \times \exp\left(8 + \frac{\Delta H_a[\mathrm{kJ\,mol^{-1}}] - 350[\mathrm{kJ\,mol^{-1}}]}{25[\mathrm{kJ\,mol^{-1}}]}\right). \quad (28)$$

However, due to their importance in kinetic models, nucleation and growth rates must be a subject of further experimental verification with different techniques and materials. In order to obtain possible thermo-kinetic coupling effects for slow slabs, we have changed the slope of the kinetic phase boundary by varying the shape factor for nucleation between 10^{-3} and 10^{-4} due to other estimates (Rubie et al., 1990; Rubie and Ross, 1994; Solomatov and Stevenson, 1994). ΔH_a is varied for fast slabs to investigate the effects of a shift of the kinetic phase boundary. According to Sung and Burns (1976), the activation energy for growth ΔG_t is the most critical parameter, which determines the shift of the kinetic phase boundary in the p–T diagram (compare Fig. 4) and in this way influences sensitively the depth of the metastable wedge. For ΔH_a we have used values between 375 kJ mol^{-1} and 450 kJ mol^{-1} (Sung and Burns, 1976; Rube et al., 1990; Rubie and Ross, 1994).

4. Results

Within the non-equilibrium framework the p-T-diagram becomes different from the equilibrium phase diagram of the olivine to spinel phase transition (Sung and Burns, 1976). First, we consider only the kinetics at the phase boundary including the time dependent p–T variation without any effects from heat diffusion (Fig. 4). Similar kinetic p–T-diagrams for the olivine to spinel phase transition and different thermal slab regimes are presented by Sung and Burns (1976), Sung (1979), Kirby et al. (1991) and Rubie and Ross (1994). The kinetic boundaries are shown as isolines, which are defined by Eq. (16) for a transformation degree of $\xi = 0.01$ and $\xi = 0.99$. They are obtained by integration of the ODE's Eq. (15) and Eq. (16) for slab velocities of 3 cm yr^{-1} and 10 cm yr^{-1} respectively. The structure of the kinetic isolines in Fig. 4 is determined by the shape factor S characterizing the heterogeneous nucleation and the free energy of growth ΔG_t, which is determined by the activation volume V^* and the activation enthalpy ΔH_a through Eq. (6). The activation volume V^* is responsible for the slope of the isolines bending towards the higher temperatures at very high pressures. In the numerical computations a value of 6 cm^3 mol^{-1} for the activation volume has been employed (Rubie and Ross, 1994). From Fig. 4(b) we observe that a shift of the kinetic phase boundary by a variation of the activation enthalpy changes the critical temperature (Sung and Burns, 1976), below which no transformation can occur. This shift also dramatically influences the transition depth inside fast slabs. For slow descending slabs ($w = 3$ cm yr^{-1}) the cold interior is heated up and the phase transformation is expected to proceed near the typical equilibrium depth at about 400 km. Due to a strong gradient of the rate functions near equilibrium, the phase transition occurs very rapidly, resulting in a sharp kinetic phase boundary. This regime is shown in Fig. 4(a), where T_a (from Fig. 3) marks the adiabat for the cold slab interior. For increasing shape factors the phase boundary shifts to greater depths and a larger metastable region results consequentely. The effects of latent-heat release on the transformation

kinetics are different between fast and slow slabs. In slow slabs, transformation occurs at p–T conditions close to the equilibrium boundary. Therefore an increase in temperature due to the latent-heat release reduces the driving force for kinetics and hence slows down the transition kinetics. On the other hand, in fast slabs, transformation occurs at p–T conditions far from the equilibrium boundary and hence an increase in temperature will enhance the transformation through the effects of thermal activation.

Taking into account the heat transfer inside the downgoing slab, the behaviour of the phase boundary now strongly depends on the slab velocity. A schematic summary of the results from the thermo-kinetic coupling is presented in Fig. 5. Within the equilibrium framework an instantaneous transformation at the equilibrium boundary with a positive Clapeyron slope is expected. Due to the temperature field, the phase transformation occurs at first in the coldest part of the subducting slab and is distorted to a shallower depth (curve E in Fig. 5). From the coupling of the transformation to the heat transfer we obtain a different behaviour near the typical depth for equilibrium (curves A and B) for slow slab velocities at about 400 km as well as for fast slabs (curves C and D) at about 600 km depth. Without latent-heat release we obtain a sharp kinetic boundary (curve A) whereas the heat release reduces the bending of the phase boundary (curve B). For fast downgoing slabs metastable olivine is shoved downward and the structure of the kinetic boundaries (curves C and D) at great depths is strongly determined by the temperature field. In this regime the gradient of the kinetic rate function changes direction and the latent-heat release intensifies the transformation process, thus pushing the metastable wedge upwards (curve C) and reducing the coexistence region of both phases in the cold slab interior.

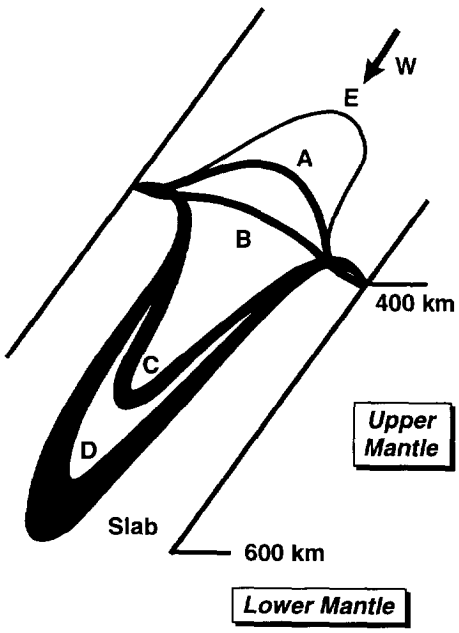

Fig. 5. Schematic summary of the thermal-kinetic effects for subducting slabs, where E marks the equilibrium boundary. A and B show schematically the kinetic phase boundaries for slow descending slabs ($w < 6$ cm yr^{-1}) without and with latent-heat release respectively. C and D illustrate schematically the kinetic phase boundaries for fast descending slabs ($w > 8$ cm yr^{-1}) with and without internal heating respectively.

In Fig. 6 the 2-D numerical results from the thermo-kinetic coupling without any latent-heat release are shown for two different slab velocities (S-slow/3 cm yr^{-1}, F-fast/10 cm yr^{-1}). The corresponding temperature fields are presented in Fig. 3. For slow slabs we obtain a narrow phase boundary with an upward distortion due to the initial p–T-field inside the slab. The sharpness of the kinetic phase boundary results from the strong nonlinearity of the rate functions near the equilibrium. For fast slabs without internal heating, we obtain large regions (> 100 km) in the cold slab interior where both phases coexist. For low values of the activation enthalpy $\Delta H_a = 375$ kJ mol^{-1} the transformation is completed within the 660 km depth-range. While the transformation in the warmer outer parts of the slab is similar to that in the slow regime, the thickness of the metastable tongue inside the slab becomes rather small at greater depths (< 10 km).

Snapshots of the temperature field and the corresponding phase boundaries for slow subducting slabs with latent-heat release are presented in Figs. 7–8 for different shape factors. Fig. 7 shows the thermal slab structure for a velocity of 3 cm yr^{-1} and an activation enthalpy of 400 kJ mol^{-1} for shape factors of 10^{-4} (Fig.

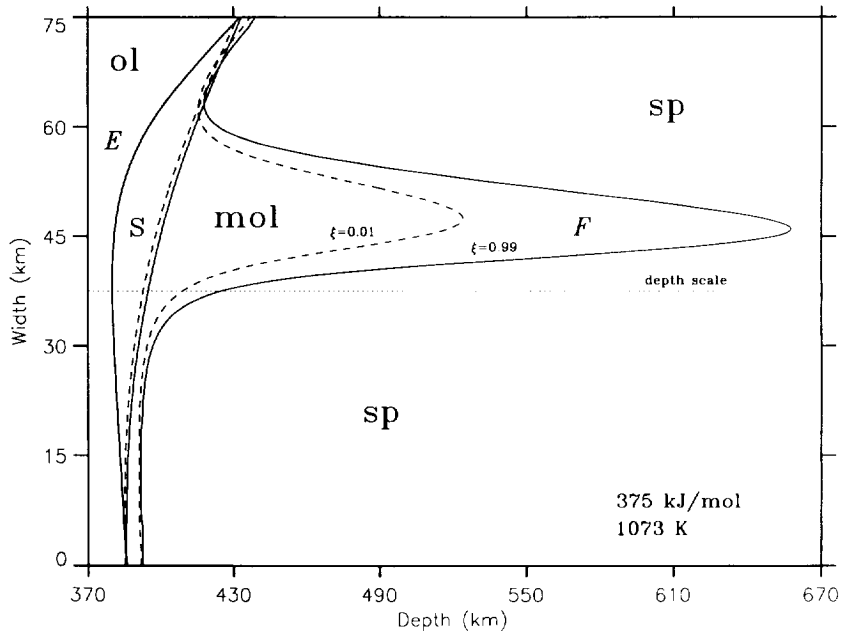

Fig. 6. Kinetic phase boundaries without latent-heat release for different slab velocity (S-slow/3 cm yr^{-1} and F-fast/10 cm yr^{-1}). The isolines mark the transformation regions between $\xi = 0.01$ (dashed line) and $\xi = 0.99$ (solid line) for an activation enthalpy of 375 kJ mol^{-1}. The slab is shown for an penetration angle of 50°. The corresponding temperature fields are shown in Fig. 3. The equilibrium line is calculated for a slab velocity of 10 cm yr^{-1}.

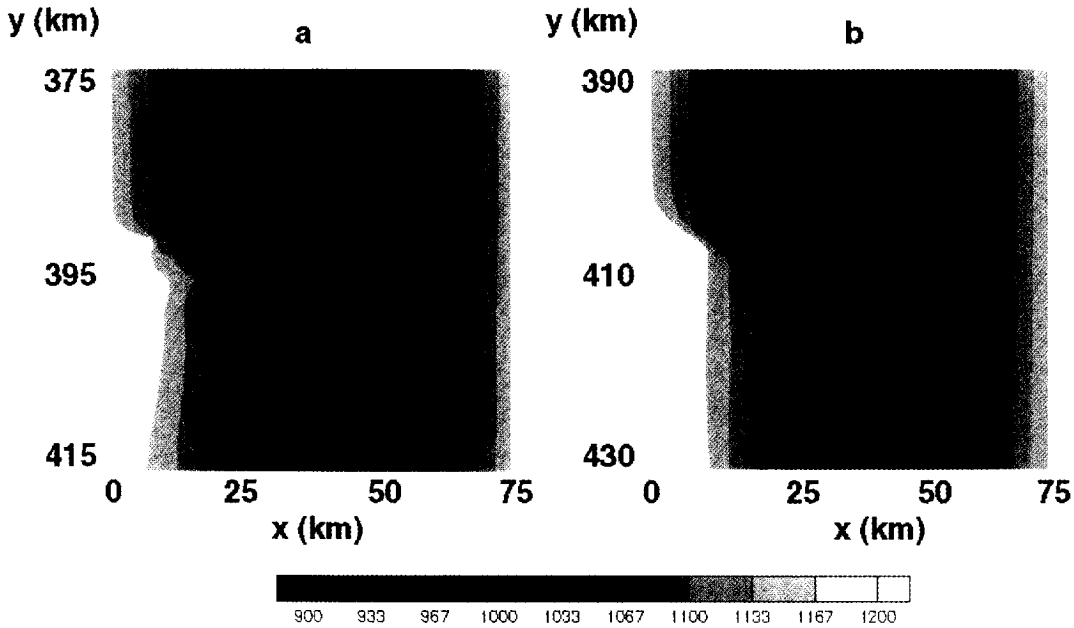

Fig. 7. Snapshots of the thermal slab structure for slowly subducting slabs (3 cm yr^{-1}) and shape factors of 10^{-4} (a) and 10^{-3} (b) respectively, both presented for an activation enthalpy of 400 kJ mol^{-1}. The corresponding temperature scale is given in K.

7(a)) and 10^{-3} (Fig. 7(b)) respectively. The corresponding phase boundaries are presented in Fig. 8, where the kinetic phase boundaries are given by the isolines of $\xi = 0.01$ and $\xi = 0.99$. The coordinate system for the following Figs. 7–10 is schematically shown in Fig. 2 as the moving system $x' - z'$. The y-axis corresponds to the depth of the centre of the slab at $x = 37.5$ km.

The latent-heat causes a heat anomaly to develop near the underneath side of the slab below the metastable wedge, which is 50–100° warmer than the surrounding lithospheric base. This development takes place because of the slow thermal diffusion compared with the kinetics. Furthermore, we obtain a significant heating of the whole slab below the sharp phase boundaries, which will modify the initial temperature field below 400 km depth. Perturbations along the corresponding phase boundaries for a lower shape factor (Fig. 8(a)) are caused by the nonlinear coupling of the kinetics and the heat transfer. However, these effects are rather small because of the small amount of latent-heat release near the equilibrium. They disappear for a higher space factor of 10^{-3} in Fig. 8(b). This can be explained by the strength of the thermal-kinetic feedback caused by a bigger kinetic slope dT/dp (see Fig. 4(a)). Because for slow slabs the transformation occurs near the typical depth for the equilibrium, one obtains a narrow boundary with only a few km thickness.

Fast subducting slabs display a completely different behaviour. The numerical results from the thermal-kinetic coupling and the effects of the latent-heat release for fast descending slabs are shown in Figs. 9–10. Fig. 9 shows the evolution of the temperature field inside a fast downgoing slab ($w = 10$ cm yr^{-1}) for an activation enthalpy of $\Delta H_a = 450$ kJ mol^{-1}. In general, there are three stages of slab penetration in the fast regime. In the outer parts of the slab the phase transition occurs near the typical depth for equilibrium (Figs. 9(a) and 10(a)), while the cold interior remains metastable. Due to the latent-heat release we obtain a small heating of both sides of the slab between 400 km and 450 km. Small amounts of heating are obtained over a long depth range (470 km and 570 km) where the

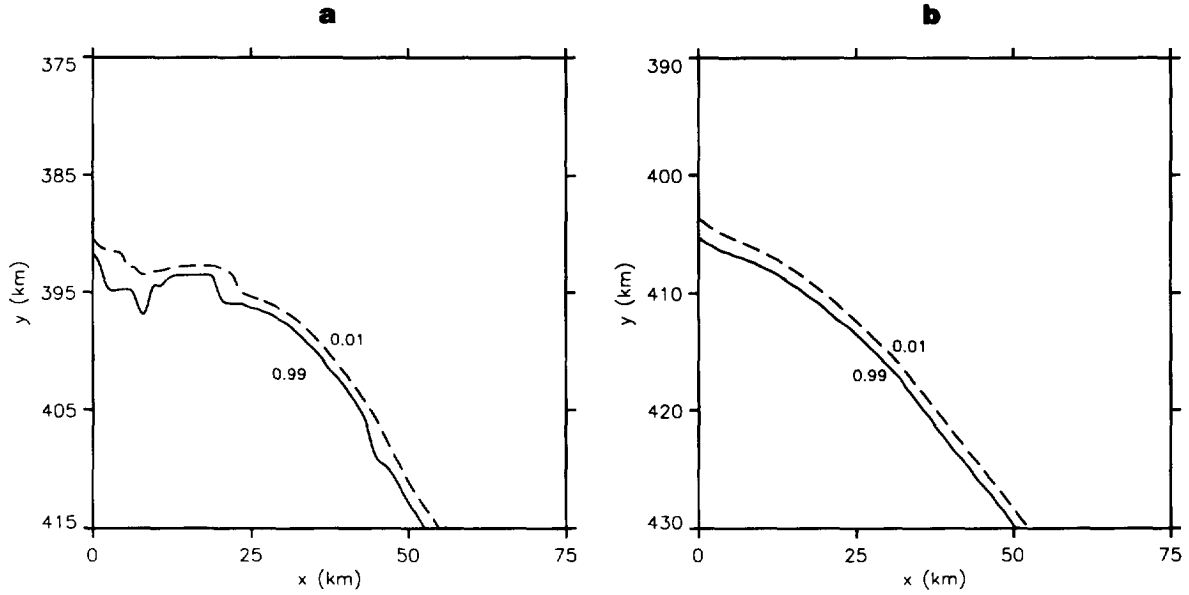

Fig. 8. Corresponding (see Fig. 7) kinetic phase boundaries for slow slabs (3 cm yr^{-1}) and shape factors of 10^{-4} (a) and 10^{-3} (b) respectively, both presented for an activation enthalpy of 400 kJ mol^{-1}. The isolines mark the transformation regions between $\xi = 0.01$ (dashed line) and $\xi = 0.99$ (solid line).

transition wedge occurs nearly parallel to the isotherms (Figs. 9(b) and 10(b)), because the gradient of the kinetic rate functions does not change much in this depth range. A small region of metastable olivine of about 10 km width (Figs. 9(c) and 10(c)) remains in the cold slab interior up to a depth of around 600 km. Latent-heat release heats up significantly the cold slab interior by the heat flow along the slab and accelerates the transition kinetics. The transformation in the cold slab interior results for a strong temperature gradient anomaly (> 150°) below the

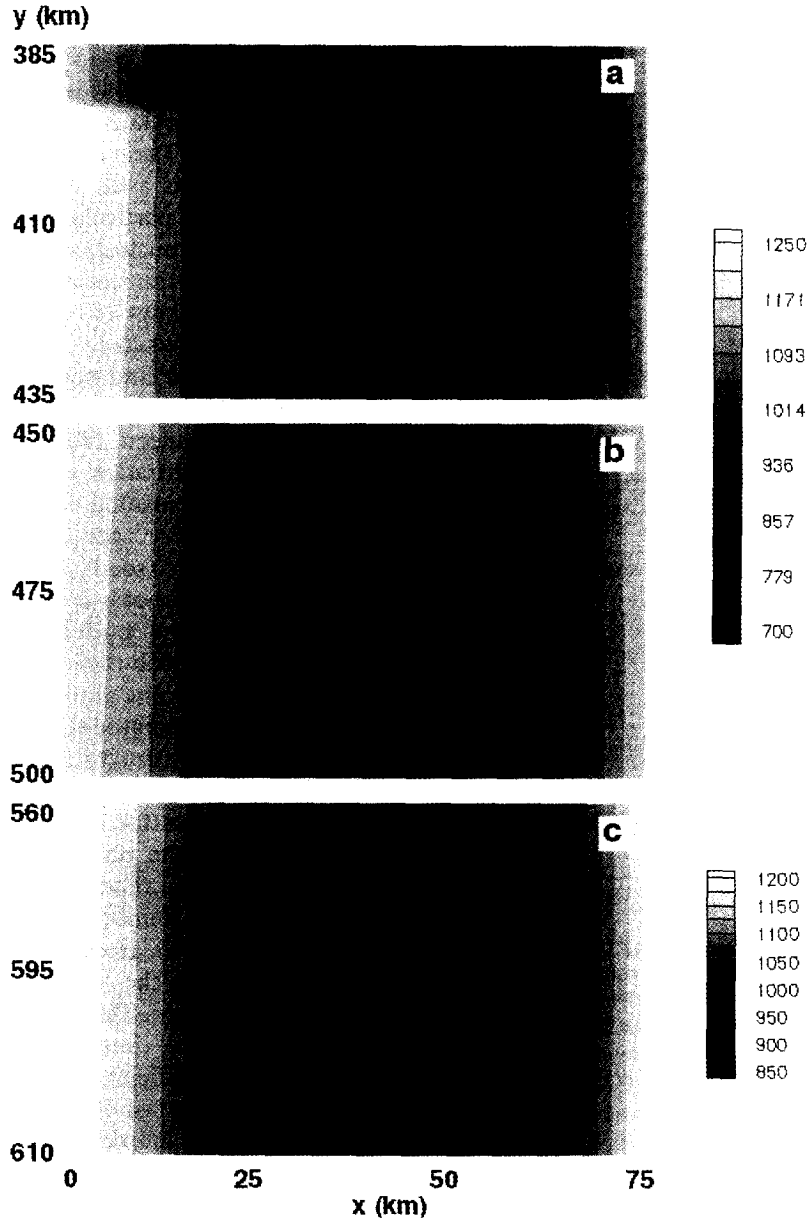

Fig. 9. Evolution of the thermal structure for a fast slab (10 cm yr^{-1}) and for an activation enthalpy of 450 kJ mol^{-1}. The evolution of the temperature field is shown at three different depths (a, b and c).

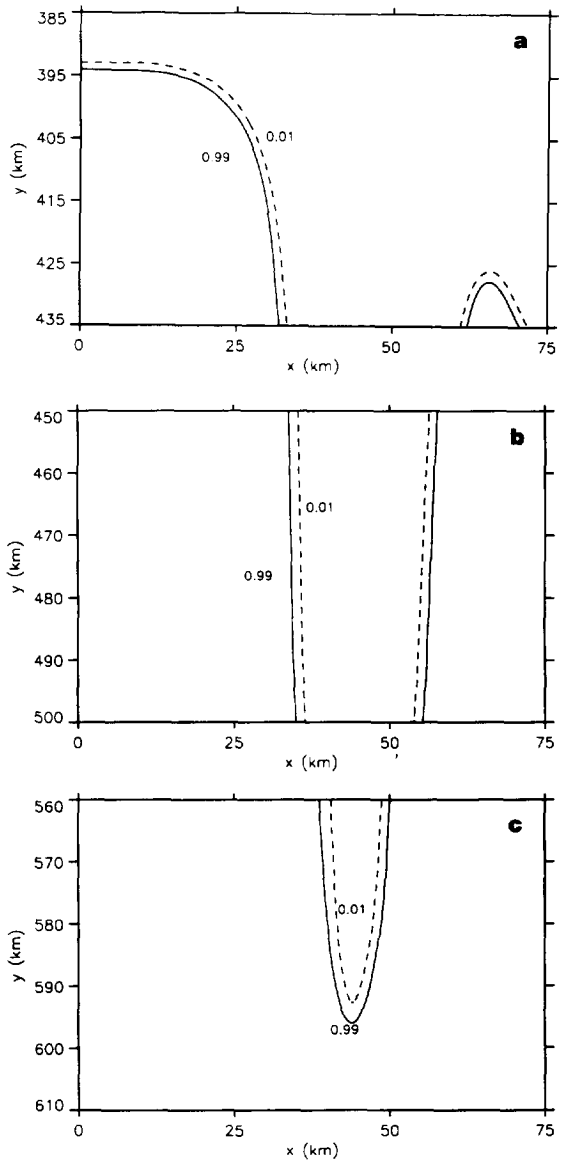

Fig. 10. Evolution of the corresponding (see Fig. 9) kinetic phase boundary for a fast slab (10 cm yr^{-1}) and for an activation enthalpy of 450 kJ mol^{-1}. The evolution of the kinetic phase boundary is shown at three different depths (a, b and c). The isolines mark the transformation regions between $\xi = 0.01$ (dashed line) and $\xi = 0.99$ (solid line).

metastable wedge (Fig. 9(c)). Additionally the thermo-kinetic coupling results in a very narrow phase boundary (Fig. 10(c)).

Table 3 summarizes parameters for the olivine–spinel phase transformation in the cold slab interior such as the maximum nucleation and growth rates, the maximum grain size and the Avrami number which characterize the transition kinetics in different slab regimes. They are obtained for a fixed grid point in the slab interior which undergoes the phase transformation during the subduction process of the slab segment by assuming a phase boundary of about 2–3 km width. For slow and warm slabs very low nucleation rates and relative high growth rates result in large grains (Table 3) and hence the transformation process is assumed to be nucleation-controlled. In this particular slab regime the estimated time for nucleation site saturation (Cahn, 1956) and the transformation time are in the same order of about 10^5 yr and hence the effect of nucleation site saturation can be neglected. In contrast, for fast and cold slabs the nucleation rates are sufficiently high but the growth rate is significantly reduced (Table 3). The estimated time for site saturation is more than one order less than the transition time. However, because the transformation process is assumed to be growth-controlled (see Rubie and Ross, 1994) the transformation process might not be significantly influenced by the nucleation regime. Furthermore in the fast slab regime we obtain in the cold interior a significant grain size reduction (about five orders of magnitude), which is in agreement with recent microstructural investigations (Riedel and Karato, 1995). The Avrami number A_v in Table 3 indicates for the different slab regimes the stability of the phase transformation due to the heat diffusion. For slow subducting slabs we obtain Avrami numbers around 10^{15} with the total slab width D. However, for a critical length of about 1 km, the thermo-kinetic interaction becomes important. Thus instabilities at the phase boundary will be caused by the thermo-kinetic coupling for a sufficiently large amount of latent-heat release. For fast descending slabs, we obtain in the cold slab interior higher Avrami numbers around 10^{19}. Therefore, in this case the critical length for instability is much smaller (10^{-2} km) than the spatial resolution and instabilities along

the metastable phase boundary are not likely to happen.

We noted that in deep portions of the slab shown in Fig. 9 (in particular (a) and (c)) there are numerical oscillations on the temperature field due to the extremes stiffness of the kinetic equations in extreme small spatial domains. In order to overcome these numerical difficulties, a higher spatial resolution is necessary. For verifying the numerical accuracy we have increased the spatial resolution by a factor of 2, which improves the accuracy of the solution. It can be shown that this will reduce the numerical oscillations of the temperature field. However, for further investigations of this particular problem the application of adaptive numerical methods (Adjerid et al., 1992) is necessary to improve the spatial resolution in the surrounding of the phase boundary.

5. Implications for deep-focus earthquakes

The present results have some potential implications for deep earthquakes. One of the possible

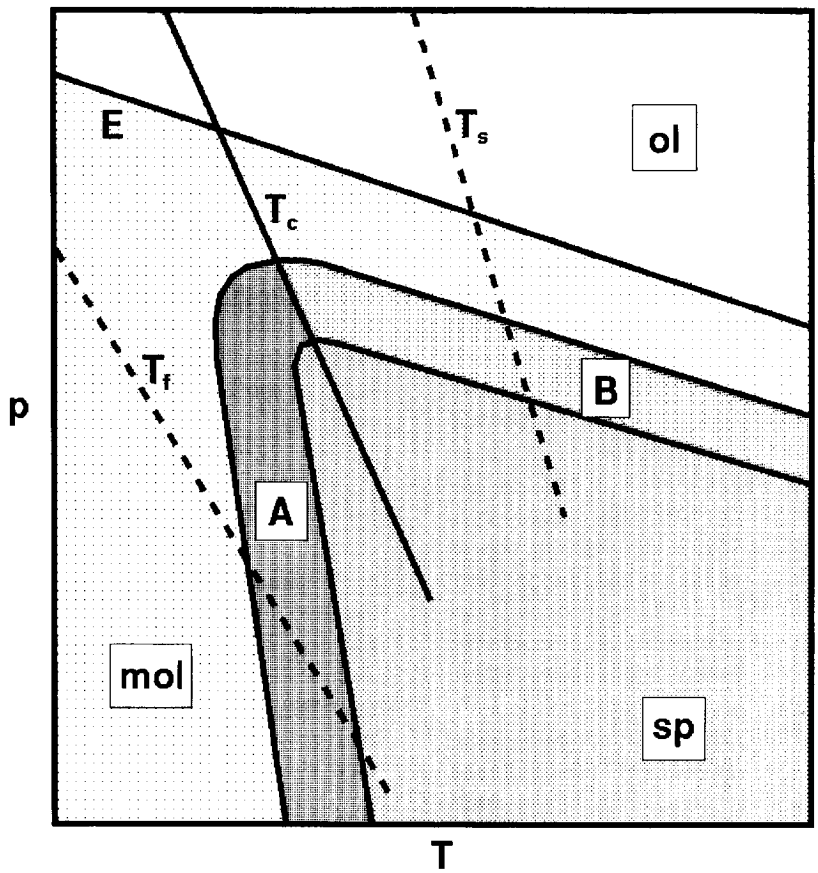

Fig. 11. A schematic diagram of the olivine–spinel phase transformation. Both equilibrium boundary (E) and kinetic boundaries for an initiation of transformation and for the completion are shown. The temperature and pressure domains are divided into five regions according to thermodynamically stable phases and to the stability of the thermal feedback associated with on-going transformations in subducting slabs (ol-stable olivine, sp-stable spinel, mol-metastable olivine, A-positive feedback, B-negative feedback). Deep earthquakes due to a thermal runaway associated with the olivine–spinel transformation could occur only for limited conditions for the thermal structure of subducting slabs. T_C, T_S and T_F are the critical adiabat and adiabats for slow and fast slabs respectively.

mechanisms of deep earthquakes is the mechanical instability associated with the olivine–spinel transformation (Kirby, 1987; Green and Burnley, 1989; Kirby et al., 1991; Green, 1994). The exact nature of instability is unknown but the recent experimental results suggest that thermal feedback due to latent-heat release plays an important role (Kirby et al., 1991; Green, 1994). The olivine–spinel transformation is exothermic and is associated with a positive latent-heat release. However, the effects of latent-heat release on the transformation kinetics depend on the temperature of a slab. In slow (warm) slabs, transformation occurs near the equilibrium boundary and therefore the change in driving force for nucleation due to latent-heat release dominates and hence the latent-heat release will retard the transforms kinetics. Thus, the latent-heat release will not lead to thermal instability in this case. In contrast, thermal instabilities due to the thermo-kinetic coupling can occur in the case where the ongoing phase transition will be enhanced by the latent-heat release causing more heat to be generated. This is obtained in relatively cold slabs where driving force term remains more or less unchanged and the effect of latent-heat is mainly through the thermal activation term. The critical condition for this stable vs. unstable transformation (with respect to the thermal instability) is the condition at which the gradient $\partial\xi/\partial T$ of the kinetics curves (i.e. the contour lines for a constant degree of transformation) changes its sign in p–T diagram (T_c; see Fig. 11): when the gradient is negative, an increase in temperature will decrease the degree of transformation and the transformation will be stable; when the gradient is positive, in contrast, the latent-heat release will increase the degree of transformation and potentially lead to thermal instability, which has a finite bound, dictated by the amount of the transition degree. In very cold slabs, no transformation will occur. Thus, we can classify the p–T domain into five regions (Fig. 11): (1) the low pressure and temperature region where olivine is thermodynamically stable, (2) the relatively low temperature region and/or regions close to the equilibrium boundary where spinel is thermodynamically stable but the formation of spinel is kinetically inhibited for a time scale of subduction, (3) the intermediate temperature domain where kinetics are fast enough to form appreciable spinel in a geological time scale and the latent-heat release causes a thermal instability, (4) the relatively high temperature and high pressure region, where transformation occurs stably and (5) the high temperature and pressure region where transformation is completed. This provides a physically reasonable explanation for Green and Burnley's (1989) observation. However, we note that the above consideration provides only the necessary conditions for instability. Another condition for instabilities is that the characteristic time for thermal diffusion is much larger than the characteristic time (Avrami time) of the phase transformation, otherwise the heat released by transformation will diffuse away and would not contribute much to a thermal instability. The time scale of thermal diffusion depends very much on the spatial scale under consideration. Therefore the nature of thermal instabilities can be very different between laboratory experiments and in the Earth. Thermal instabilities are prone to occur in the Earth more than in laboratory experiments because of the much larger spatial scale in the Earth.

6. Discussion and conclusions

In summarizing the results we much consider the two end-member cases involving both slow and fast subduction, which result in distinct differences of the structure of the kinetic phase boundary. Each of the regimes causes a different heating response in the slab. Hence, this difference results in a completely different behaviour at the point where p–T paths cross the kinetic phase boundary (see Fig. 4). Because of the opposite gradients of the kinetic curves in both regimes, the latent-heat release drives the kinetics in fast slabs or conversely hinders the kinetics in slow slabs (Kirby et al., 1991). The structure of the kinetic phase boundary can therefore be strongly determined by thermo-kinetic coupling effects during the transition.

For slow, warm slabs near 400 km a large spatial temperature anomaly is obtained, resulting from the heat release during the transformation. Because of the small latent-heat release near the equilibrium (< 10 kJ mol^{-1}), the increase in temperature is rather small (50–100°). In different slow regimes the kinetic phase boundary is found to be very narrow. Thermo-kinetic coupling effects which significantly influence the structure of the kinetic phase boundary by a negative thermo-kinetic feedback are not likely for the α–β transition but may play an important role during the β–γ transition associated by a much larger latent-heat release (Chopelas et al., 1994)

For fast, cold slabs regions with metastable olivine may be pushed down to a depth of about 600 km within the considered parameter space. We have found a high sensitivity of the depth of the metastable wedge on transition parameters, such as activation energy. The latent-heat release associated with the phase transformation results in two different effects: a heating along both sides of the slab near 400 km and a much stronger heating (100–150°) of the cold slab interior at greater depths. The verification of such temperature anomalies inside slabs at this time is very difficult and requires a high-resolution seismic tomography (Zhou, 1990). Thermo-kinetic coupling effects drastically reduce the coexistence region of the olivine and spinel phase and they decrease the depth of the metastable wedge. Although, for certain thermodynamic parameters the olivine–spinel transition is obtained at great depths, the metastable region becomes very narrow (see Fig. 10(c)) and hence the retarding effect to the slab motion is reduced. The predicted depths of the metastable wedge might drastically change by using different thermal slab models because of the high sensitivity to the thermal structure.

Deep-focus earthquakes may occur because of the sharp tapering of the metastable phase boundary near 600 km depth accompanied with a rapid and localized heating of the cold slab interior. If metastable olivine does not deeply penetrate, because of the slab heating, other metastable transitions such as enstatite to ilmenite (Hofgrefe et al., 1994) might be investigated for the origin of deep-focus earthquakes at greater depths.

Our results agree with previous speculations concerning the structure of subducting slabs due to the presence of metastable olivine (Kirby et al., 1991), with new seismic investigations of the seduction zone (Vidale and Benz, 1992; Houston, 1993) and recent thermo-kinetic models (Däßler and Yuen, 1993; Rubie and Ross, 1994; Solomatov and Stevenson, 1994). The internal heating due to metastable phase changes, the viscous heating along both sides of the slab (Larsen et al., 1995) as well as effects of grain size reduction (Riedel and Karato, 1995) all help to reduce dramatically the strength of subducting slabs which in turn would influence their fate.

This model has some limitations. An isochemical subsystem is considered where the strain energy ϵ due to the phase mismatch (Eq. (7)) is neglected and the effects of deformation are not considered. The thermal interaction between mantle and descending slab is simplified by Eq. (27). The temperature field inside the downgoing slab segment may be influenced by the adiabatic boundary conditions especially along the bottom of the slab segment. Our model may therefore overestimate the heating inside the slab. On the contrary, we have neglected any external heating of the slab. From our modeling we obtain very narrow phase boundaries for both slow and fast subduction processes. This sharpness of the metastable region in the fast slab regime may result from overestimated magnitudes of the rates of nucleation caused by neglecting the effects of site saturation during the heterogeneous nucleation process. While this 2-D approach shows for the first time the potentially important effects of the thermo-kinetic coupling associated with downgoing slabs, longer integration times up to 100 Ma for the thermal evolution of the entire slab would give a better understanding of the dynamics in older slabs.

In this work we have shown that kinetic effects in phase transitions can exert significant influences in descending slabs. It has been shown that phase transition kinetics can play an important role in mantle dynamics in two ways: as a mecha-

nism generating deep focus earthquakes and as a driving mechanism for sinking lithospheric slabs in plate tectonics. The phase boundaries inside a slab are influenced by many factors. Important factors found in this study are the magnitude of the surface energy and the magnitude of activation energy. These parameters should be determined more precisely in future experimental work. Another important contributor is the descending velocity of the slab. For fast descending slabs, the metastable region can be maintained down to great depths, very close to the spinel to perovskite phase change. This region of metastability gets thinner with depth with a tongue-like structure. There seems to be for some slabs a correlation between the distribution of earthquakes and the subducting plate velocity (Table 4). In the Tonga–Kermadec region, there is a strong cluster of earthquakes at 600 km depth and the descending velocity of the Tonga trench is close to 10 cm yr^{-1}. On the other hand, for slower descending slabs such as the Izu–Bonin trench there is a clustering of the earthquake distribution at around 400 km depth (Wicks and Richards, 1993) and the local plate velocity is relatively slow there.

What are some implications for the driving force fo subduction? Metastable olivine phase boundaries will give rise to a significant reduction of the driving force for descending slabs and also a hot and weaker slab interior. A hot and weak slab would have greater difficulty in penetrating the 660 km discontinuity. These theoretical calculations suggest that the depth to which metastable olivine will persist depends very much on the slab temperature and assumed thermodynamic parameters, which are still highly uncertain. However, some general trends appear to be robust by including the deeper depth of transformation for a faster slab. The dependence of the depth of phase transition on the slab velocity has important implications for the driving force for subduction. Slowly subducting slabs will tend to have shallower depth of transformation, and hence the effect of metastable olivine to reduce the driving force is small. In contrast, in a fast subducting slab where the metastable olivine might be dragged deeply into the mantle, there would be a strong resistance to subduction from the metastable olivine. Therefore, there will be a stabilizing effect. The same effect also would hold for the metastable spinel to perovskite transition.

Acknowledgements

We thank Slava Solomatov for his helpful discussions and Linda Petzold, Werner Rath and Jamie Smedsmo for help in implementing DASPK. We thank Prof. U. Bayer for his support in computation. This research was supported by the Deutscher Akademischer Austauschdienst Deutschland (DAAD), the Geosciences program of DOE and the National Science Foundation (Geophysics and Geochemistry programs).

Appendix

The system of coupled ordinary differental equations (Eq. (15)) can be derived by the differ-

Table 4
Examples for subductions zones, where the model is applicable (taken from Burbach and Frohlich, 1986)

Subduction zone	Approx. subduction rate in cm yr^{-1}	Approx. dip angle in degrees	Approx. depth of deep earthquakes in km
Kamchatka	6	40	400
Izu–Bonin	5–6	60	400
Tonga–Kermandec	8–12	60	670
Solomon–New Hebrides	7–10	70	670
Java	7	70	670

entiation of Kirkpatricks formula (Eq. (3)), given in the extended volume formulation:

$$X_3(t) = \frac{4\pi}{3}\int_0^t I(t_1)\left[\int_{t_1}^t Y(t_2)\,dt_2\right]^3 dt_1. \quad (29)$$

The derivative of $X_3(t)$ in time is given by

$$\frac{d}{dt}X_3(t) = \frac{4\pi}{3}\int_0^t I(t_1)\frac{\partial}{\partial t}\left[\int_{t_1}^t Y(t_2)\,dt_2\right]^3 dt_1 + \frac{4\pi}{3}I(t)\left[\int_t^t Y(t_2)\,dt_2\right]^3. \quad (30)$$

We introduce now the new variable $X_2(t)$ with

$$X_2(t) = \int_0^t I(t_1)\left[\int_{t_1}^t Y(t_2)\,dt_2\right]^2 dt_1. \quad (31)$$

From Eq. (30) one can write

$$\frac{d}{dt}X_3(t) = 4\pi Y(t)X_2(t). \quad (32)$$

The derivative of $X_2(t)$ in time is given by

$$\frac{d}{dt}X_2(t) = \int_0^t I(t_1)\frac{\partial}{\partial t}\left[\int_{t_1}^t Y(t_2)\,dt_2\right]^2 dt_1 + I(t)\left[\int_t^t Y(t_2)\,dt_2\right]^2. \quad (33)$$

We introduce now the new variable $X_1(t)$ with

$$X_1(t) = \int_0^t I(t_1)\left[\int_{t_1}^t Y(t_2)\,dt_2\right] dt_1. \quad (34)$$

From Eq. (33) it follows that

$$\frac{d}{dt}X_2(t) = 2Y(t)X_1(t). \quad (35)$$

The derivative of $X_1(t)$ in time is given by

$$\frac{d}{dt}X_1(t) = \int_0^t I(t_1)\frac{\partial}{\partial t}\left[\int_{t_1}^t Y(t_2)\,dt_2\right] dt_1 + I(t)\int_t^t Y(t_2)\,dt_2. \quad (36)$$

We introduce now the new variable $X_0(t)$ with

$$X_0(t) = \int_0^t I(t_1)\,dt_1. \quad (37)$$

The derivative of $X_1(t)$ leads to

$$\frac{d}{dt}X_1(t) = Y(t)X_0(t). \quad (38)$$

and the derivative of $X_0(t)$ is given by the nucleation rate

$$\frac{d}{dt}X_0(t) = I(t). \quad (39)$$

References

Adjerid, S., Flaherty, J.E., Moore, P.K. and Wang, Y.J., 1992. High-order adaptive methods for parabolic systems. Physica D, 60: 94–111.

Akaogi, M., Ito, E. and Navrotsky, A., 1989. Olivine–modified spinel–spinel transitions in the system Mg_2SiO_4–Fe_2SiO_4: Calorimetric measurements, thermochemical calculation, and geophysical application. J. Geophys. Res. B, 94: 15671–15685.

Avrami, M., 1939. Kinetics of phase change. I. General theory. J. Chem. Phys., 7: 1103–112.

Avrami, M., 1940. Kinetics of phase change. II. Transformation-time relations for random distribution of nuclei. J. Chem. Phys., 8: 212–224.

Avrami, M., 1941. Kinetics of phase change. III. Granulations, phase change, and microstructure. J. Chem. Phys., 9: 177–184.

Axe, J.D. and Yamada, Y., 1986. Scaling relations for grain autocorrelation functions during nucleation and growth. Phys. Rev. B, 34: 1599–1606.

Bassett, W.A., 1979. The diamond cell and the nature of the earth's mantle. Ann. Rev. Earth Planet. Sci., 7: 357–384.

Brandeis, G., Jaupart, C. and Allegre J., 1984. Nucleation, crystal growth and the thermal regime of cooling magmas. J. Geophys. Res. B12, 89: 10161–10177.

Brearley, A.J., Rubie, D.C. and Ito, E., 1992. Mechanisms of the transformations between the α, β and γ polymorphs of Mg_2SiO_4 at 15 GPA. Phys. Chem. Minerals, 18: 343–358.

Brenan, K.E., Campbell, S.L. and Petzold, L.R., 1989. Numerical Solution of Initial-value problems in differential-algebraic Equations. Elsevier, New York.

Burbach, G.V. and Frohlich, C., 1986. Intermediate and deep seismicity and lateral structure of subducted lithosphere in the Circum–Pacific area. Rev. Geophys., 24: 833–874.

Cahn, J.W., 1956. The kinetics of grain boundary nucleated reactions. Acta Metall., 4: 449–459.

Carlson, W.D., 1983. Aragonite–calcite nucleation kinetics: An application and extension of Avrami transformation theory. Nature, 338: 753–756.

Chopelas, A. and Boehler, R., 1994. Thermodynamics and behavior of γMg_2SiO_4 at high pressure: Implications for

Mg_2SiO_4 phase equilibrium. Phys. Chem. Min., (1994) 351–359.

Christian, J.W., 1965. The Theory of Transformations in Metals and Alloys. Pergamon, New York.

Däßler, R., 1990. Kinetics of pressure-induced nucleation and growth processes in the diamond anvil cell. High Temp. High Press., 22: 599–612.

Däßler, R. and Yuen, D.A., 1993. The effects of phase transition kinetics on subducting slabs. Geophys. Res. Lett., 20: 2603–2606.

Däßler, R. and Yuen, D.A., 1994. Two-dimensional modeling of thermal-kinetics coupling. EOS, American Geophysical Union Transactions, 75: 679–680.

Dowty, E., 1980. Crystal growth and nucleation theory and the numerical simulation of igneous crystallization. In: R.B. Hargraves (Editor), Physics of Magmatic Processes, Princeton University Press, pp. 419–485.

Frohlich, C., 1994. A break in the deep. Nature, 368: 100–101.

Fujino, K. and Irifune, T., 1992. TEM studies on the olivine to modified spinel transformation in Mg_2SiO_4. In: Y. Syono and M.H. Manghnani (Editors), High Pressure Research: Application to Earth and Planetary Sciences, Terra Sci. Pub., (AGU): 237–243.

Furukawa, Y., 1994. Two types of seismicity in subducting slabs. Geophys. Res. Lett., 21: 1181–1184.

Goto, K., Suzuki, Z. and Hamaguchi, H., 1987. Stress distribution due to olivine–spinel phase transition in descending plate and deep-focus earthquakes, J. Geophys. Res. B, 92: 13811–13820.

Green, H., 1994. Solving the paradox of deep earthquakes. Sci. Am., 271: 64–71.

Green, H.W. and Burnley, P.C., 1989. A new self-organizing mechanism for deep-focus earthquakes. Nature, 341: 733–737.

Griggs, D.T., 1972. The sinking lithosphere and the focal mechanism of deep earthquakes. In: E.C. Robertson, J.F. Hays and L. Knopoff (Editors), The Nature of the Solid Earth, McGraw-Hill, New York, pp. 361–384.

Griggs, D.T. and Baker, D.W., 1969. The origin of deep-focus earthquakes. In: S. Fernbach (Editor), Properties of Matter Under Unusual Conditions, Wiley, New York, pp. 23–41.

Hamaya, N. and Akimoto, S., 1982. Experimental investigation on the mechanism of olivine → spinel transformation: Growth of single crystal spinel from single crystal olivine in Ni_2SiO_4. In: S. Akimoto and M.H. Manghnani (Editors), High Pressure Research in Geophysics, D. Reidel, Hingham, Massachusetts, pp. 373–389.

Hofgrefe, A., Rubie, D.C., Sharp, T.G. and Seifert, F., 1994. Metastability of enstatite in deep subducting lithosphere. Nature, 372: 351–353.

Honda, S., Yuen, D.A., Balachandar, S. and Reuteler, D., 1993. Three-dimensional instabilities of mantle convection with multiple phase transitions. Science, 259: 1308–1311.

Houston, H., 1993. The non-double-couple component of deep earthquakes and the width of the seismogenic zone. Geophys. Res. Lett, 20: 1687–1690.

Hsui, A.R. and Toksöz, M.N., 1979. The evolution of thermal structures beneath a subduction zone. Tectonophysics, 60: 43–60.

Jeanloz, R. and Thompson, A.B., 1983. Phase transitions and mantle discontinuities. Rev. Geophys. Space Phys., 21: 51–74.

Johnson, W.A. and Mehl, R.F., 1939. Reaction kinetics in processes of nucleation and growth. Trans. Am. Inst. Min. Metall. Eng., 135: 416–458.

Kirby, S.H., 1987. Localized polymorphic phase transformations in high-pressure faults and applications to the physical mechanism of deep earthquakes. J. Geophys. Res., 92: 13789–13800.

Kirby, S.H., Durham, W.B. and Stern L.A., 1991. Mantle phase changes and deep-earthquake faulting in subducting lithosphere. Science, 252: 216–225.

Kirkpatrick, R.J., 1976. Towards a kinetic model for the crystallization of a magma body. J. Geophys. Res., 81: 2565–2571.

Larsen, T., Yuen, D.A. and Malevsky, A.V., 1995. Dynamical consequences on fast subducting slabs from a self-regulating mechanism due to viscous heating in variable viscosity convection. Geophys. Res. Lett., 22: 1277–1280.

Machetel, P. and Weber, P., 1991. Intermittent layered convection in a model mantle with an endothermic phase change at 670 km. Nature, 350: 55–57.

Maier, R.S. and Petzold, L.R., 1993. User's guide to DASPKMP and DASPKF90. AHPCRC Reprint 93-034, University of Minnesota, Minneapolis, MN.

McKenzie, D.P., 1969. Speculations on the consequences and causes of plate motions. Geophys. J.R. Astron. Soc., 18: 1–32.

Minear, J.W. and Toksöz, M.N., 1970. Thermal regime of downgoing slabs. Tectonophysics, 10: 367–390.

Morris, S., 1992. Stress relief during solid-state transformations in minerals. Proc. R. Soc. London A, 436: 203–216.

Ogawa, M., 1987. Shear instability in a viscoelastic material as the cause of deep focus earthquakes. J. Geophys. Res. B, 92: 13801–13810.

Peltier, W.R. and Solheim, L.P., 1992. Mantle phase transition and layered chaotic convection. Geophys. Res. Lett., 19: 321–324.

Riedel, M. and Däßler, R., 1990. Pressure-induced nucleation and growth processes in the diamond anvil cell. J. Crystal Growth, 106: 695–704.

Riedel, M. and Karato, S., 1995. Microstructural development during nucleation and growth. Geophys. J. Int., in press.

Rubie, D.C. and Ross, C.R., 1994. Kinetics of the olivine–spinel transformation in subducting lithosphere: experimental constraints and implications for deep slab processes. Phys. Earth Planet. Inter., 86: 223–241.

Rubie, D.C., Tsuchida, Y., Yagi, T., Utsumi, W., Kikegawa, T., Shimomura, O. and Brearley, A.J., 1990. An in-situ x-ray diffraction study of the kinetics of the Ni_2SiO_4 olivine–spinel transformation. J. Geophys. Res. B, 95: 15829–15844.

Sigsbee, R.A., 1969. Vapour to condensed-phase heteroge-

neous nucleation. in: A.C. Zettlemoyer (Editor), Nucleation, Dekker, New York, pp. 152–224.

Solomatov, V.S. and Stevenson, D.J., 1993. Kinetics of crystal growth in a terrestrial magma ocean. J. Geophys. Res. E, 98: 5407–5418.

Solomatov, V.S. and Stevenson, D.J., 1994. Can sharp seismic discontinuities be caused by non-equilibrium phase transformations? Earth Planet. Sci. Lett., 125: 267–279.

Spohn, T., Hort, M. and Fischer, H., 1988. Numerical simulation of the crystallization of multicomponent melts in thin dikes or sills. I. The liquidus phase. J. Geophys. Res., 93: 4880–4894.

Steinbach, V., Yuen, D.A. and Zhao, W., 1993. Instabilities from phase transitions and the timescales of mantle evolution. Geophys. Res. Lett., 20: 1119–1122.

Sung, C.M., 1979. Kinetics of the olivine–spinel transition under high pressure and temperature: Experimental results and geophysical implications. In: K.D. Timmerhaus and M.S. Barber (Editors), High Pressure Science and Technology, Vol. 2, Plenum Press, pp. 31–42.

Sung, C.M. and Burns, R.G., 1976. Kinetics of high pressure phase transitions: Implications to the evolution of the olivine–spinel transition in the downgoing lithosphere and its consequences on the dynamics of the mantle. Tectonophysics, 31: 1–32.

Tackley, P.J., Stevenson, D.J., Glatzmaier, G.A. and Schubert, G., 1993. Effects of an endothermic phase transition at 670 km depth in a spherical model of convection in the Earth's mantel. Nature, 361: 699–704.

Turcotte, D.L. and Schubert, G., 1982. Geodynamics. Applications of Continuum Physics to Geological Problems. Wiley, New York, 437 pp.

Vidale, E. and Benz, M., 1992. Upper mantle seismic discontinuities and the thermal structure of subduction zones. Nature, 356: 678–683.

Wicks, C.W. and Richards, M.A., 1993. A detailed map of the 660 km discontinuity beneath the Izu–Bonin subduction zone. Science, 261: 1424–1427.

Zhou, H., 1990. Observations on earthquake stress axes and seismic morphology of deep slabs. Geophys. J. Int., 103: 377–401.